Numerical Simulation of a Solar Domestic Hot Water System



2014 J. Phys.: Conf. Ser. 547 012015

(http://iopscience.iop.org/1742-6596/547/1/012015)

Journal of Physics: Conference Series **547** (2014) 012015 doi:10.1088/1742-6596/547/1/012015

# Numerical Simulation of a Solar Domestic Hot Water System

**L Mongibello[1], N Bianco[2], M Di Somma[2], G Graditi[1], V Naso[2]**

[1] ENEA – Italian National Agency for New Technologies, Energy and Sustainable Economic Development, Portici RC – Napoli – Italy
[2] Dipartimento di Ingegneria Industriale (DII) – Università degli Studi Federico II – Napoli – Italy

**Abstract.** An innovative transient numerical model is presented for the simulation of a solar Domestic Hot Water (DHW) system. The solar collectors have been simulated by using a zero-dimensional analytical model. The temperature distributions in the heat transfer fluid and in the water inside the tank have been evaluated by one-dimensional models. The reversion elimination algorithm has been used to include the effects of natural convection among the water layers at different heights in the tank on the thermal stratification. A finite difference implicit scheme has been implemented to solve the energy conservation equation in the coil heat exchanger, and the energy conservation equation in the tank has been solved by using the finite difference Euler implicit scheme. Energy conservation equations for the solar DHW components models have been coupled by means of a home-made implicit algorithm. Results of the simulation performed using as input data the experimental values of the ambient temperature and the solar irradiance in a summer day are presented and discussed.

## 1. Introduction

The production of Domestic Hot Water (DHW) by means of non-concentrating solar thermal collectors is one of the most efficient and cost effective ways to utilize the solar energy.

In the last decades, several papers have focused on transient mathematical models of solar DHW systems. Rodriguez-Hidalgo et al. [1] developed and validated experimentally a transient model in order to achieve the design criteria of solar DHW systems under daily transient conditions. Dehghan et al. [2] investigated numerically the transient performance of a solar DHW system including a vertical storage tank with a mantle heat exchanger. Kenjo et al. [3] modeled the mantle tank of a solar DHW system by using a zonal approach, and they validated the model with experimental tests.

Several transient models of the components of solar DHW systems have been proposed. Klein et al. [4] studied numerically the effects of the thermal capacitance on the performance of a flat plate solar collector. Rodriguez-Hidalgo et al. [5, 6] investigated the efficiency of a flat plate solar collector by using a transient zero-dimensional mathematical model. Cadafalch [7] analysed different configurations of a flat-plate solar collector using a one-dimensional transient numerical model. Transient mathematical models for solar DHW systems were also proposed by Logie et al. [8] and Chauvet et al. [9].

This paper is focused on the numerical simulation of a solar DHW system consisting of two flat plate collectors connected in series, a vertical cylindrical water tank for the heat storage, and a coil heat exchanger immersed into the water tank. The performance of the system has been simulated using a Matlab home-made code. The temperature distributions in the heat transfer fluid and in the water

inside the tank have been evaluated by unsteady one-dimensional models. The reversion elimination algorithm has been used to include the effects of natural convection among the water layers at different heights in the tank on the thermal stratification. In the first part of the paper, the analytical models, the numerical schemes and the algorithms used in the simulation are reported in detail. In the second part, results of the simulation performed using as input data the measured values of the ambient temperature and the solar irradiance in a summer day are presented and discussed.

## 2. Models of the solar DHW system components

Figure 1 shows the sketch of the investigated system.

### *2.1. Solar collector model*

In the present study reference is made to a couple of commercial flat-plate solar collectors Vitosol 100 w2.5 by Viessmann Werke GmbH and Co KG®. Table 1 reports their main data. The collectors were assumed to be connected in series and installed in Portici (Italy), due south, with a 30° inclination above the horizontal. The wind velocity was assumed to be equal to zero and a solution of water and propylene glycol (30%) was considered as the heat transfer fluid (HTF).

A zero-dimensional analytical model has been developed to evaluate the time-variable temperature of the collectors components and the temperature of the HTF at the exit sections of the collectors. Figure 2 shows a sketch of the collector cross section and the thermal circuit for the lumped-element model that has been used to carry out the energy balances. The conductive thermal resistances of the box aluminum back cover, the glass, the copper absorber plate were neglected, since they are negligible compared with the insulation thermal resistance.

With reference to figure 2, the following correlations hold for each collector.

The energy balance on the collector insulation gives

$$\frac{T_{abs} - T_{ins,coll}}{R_{ins,coll}} - \frac{T_{ins,coll} - T_{box}}{R_{ins,coll}} = c_{ins,coll}\, \rho_{ins,coll}\, A_{ins,coll}\, L_{ins,coll}\, \frac{d\left(T_{ins,coll}\right)}{dt} \qquad (1)$$

where $T_{abs}$ and $T_{box}$ are the temperatures of the absorber plate and the box back cover, respectively; $T_{ins,coll}$ is the lumped temperature of the insulation; $c_{ins,coll}$, $\rho_{ins,coll}$, $L_{ins,coll}$, are the specific heat, the density, the thickness of the insulation, respectively, $t$ is the time; and the insulation thermal resistance, $R_{ins,coll}$, is given by

$$R_{ins,coll} = (L_{ins,coll}/2)\left(A_{ins,coll}\, k_{ins,coll}\right)^{-1} \qquad (2)$$

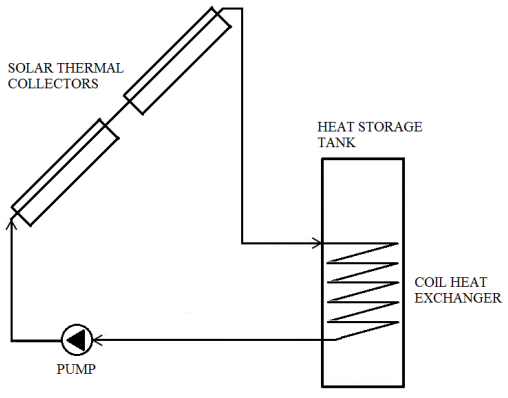


**Figure 1.** Sketch of the solar DHW system.

**Table 1.** Collector data.

| |
|---|
| Collector width: 2.39 m; Collector length: 1.14 m |
| Absorber plate area: 2.50 $m^2$ |
| Glass cover thickness: 4.0 $10^{-3}$ m |
| Inner air layer thickness: $2.6 \cdot 10^{-2}$ m |
| Absorber sheet thickness (Cu): $2.5 \cdot 10^{-4}$ m |
| Outer tube diameter (Cu): $1.0 \cdot 10^{-2}$ m |
| Inner tube diameter (Cu): $8.0 \cdot 10^{-3}$ m |
| Insulation thickness (mineral fiber): $5.0 \cdot 10^{-2}$ m |
| Box back cover thickness (Al): $2.0 \cdot 10^{-3}$ m |
| Glass emittance: 0.85; Glass transmittance: 0.90 |
| Absorber plate emittance: 0.70 |
| Absorber plate absorptance: 0.94 |

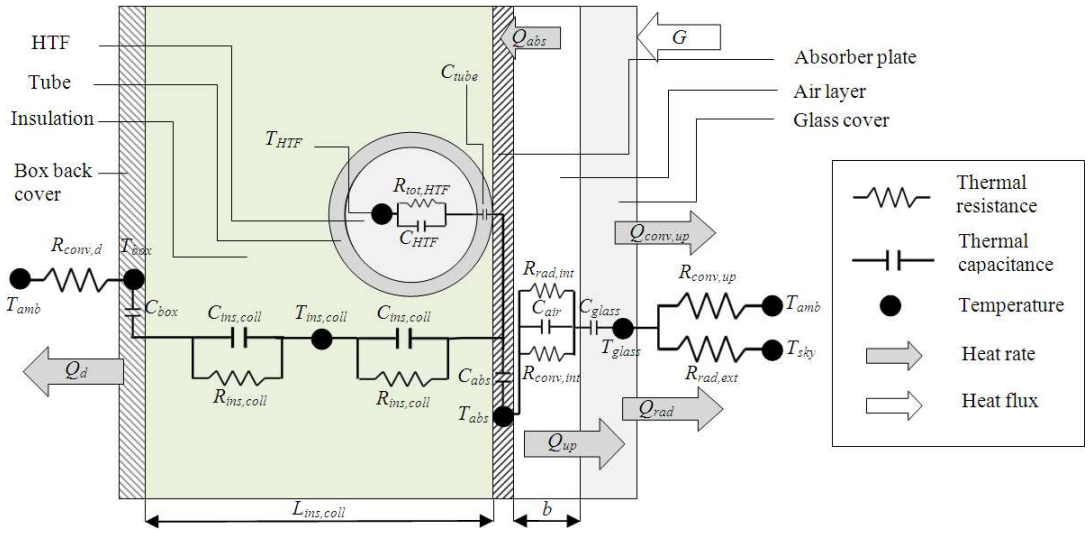


**Figure 2.** Cross section and thermal circuit of the collector.

with $A_{ins,coll}$ the insulation section area; $k_{ins,coll}$ the insulation thermal conductivity.

The heat rate dissipated through the box back cover, $Q_d$, is

$$Q_d = (T_{box} - T_{amb}) \left(R_{conv,d}\ \right)^{-1} \tag{3}$$

where $T_{amb}$ is the ambient air temperature and the convective thermal resistance at the box back cover surface, $R_{conv,d}$, is given by

$$R_{conv,d} = 1/\left(\ A_{box}\ \bar{h}_{conv,d}\right) \tag{4}$$

with $A_{box}$ the area of the box back surface in contact with the air and $\bar{h}_{conv,d}$ the mean convective heat transfer coefficient at the box back surface, evaluated as in [10].

$$R_{int}\ Q_{up} = T_{abs} - T_{glass} \tag{5}$$

where $Q_{up}$ is the heat rate transferred by the absorber plate to the glass, $T_{glass}$ is the temperature of the glass and the thermal resistance of the enclosure between the absorber plate and the glass cover, $R_{int}$, accounts for the parallel contributions of radiation and convection in the enclosure

$$R_{int} = \left(R_{rad,int}^{-1} + R_{conv,int}^{-1}\right)^{-1} \tag{6}$$

The internal radiative thermal resistance, $R_{rad,int}$, assuming the surfaces to be grey, is given by

$$R_{rad,int} = \left(1/\varepsilon_{glass}\ \varepsilon_{abs}\right)\left[\sigma\ A_{abs}\left(T_{glass}^2 + T_{abs}^2\right)\left(T_{glass} + T_{abs}\right)\right]^{-1} \tag{7}$$

where $\varepsilon_{glass}$ and $\varepsilon_{abs}$ are the emittancies of the glass and the absorber plate surfaces, respectively; $\sigma$ is the Stephan-Boltzmann constant; $A_{abs}$ is the absorber plate area.

The internal convective thermal resistance, $R_{conv,int}$, is given by

$$R_{conv,int} = 1/\left(\ A_{abs}\ \bar{h}_{conv,int}\right) \tag{8}$$

where $\bar{h}_{conv,int}$ is the mean natural convective heat transfer coefficient in the enclosure

$$\bar{h}_{conv,int} = \left(\overline{Nu}_{air}\ k_{air}\right)\ b^{-1} \tag{9}$$

with $\overline{Nu}_{air}$ the mean Nusselt number evaluated using the Hollands et al. correlation [11]; $k_{air}$ the

thermal conductivity of the air; *b* the enclosure thickness.

The convective heat rate from the glass to the ambient air, $Q_{conv,up}$, is given by

$$Q_{conv,up} = \left(T_{glass} - T_{amb}\right)/R_{conv,up} \tag{10}$$

where the convective thermal resistance at the glass cover surface, $R_{conv,up}$, is given by

$$R_{conv,up} = 1/\left(A_{abs}\,\bar{h}_{conv,up}\right) \tag{11}$$

with $\bar{h}_{conv,up}$ the mean convective heat transfer coefficient at the glass surface, evaluated as in [10].

The radiative heat rate from the glass to the ambient, $Q_{rad}$, is given by

$$R_{rad,ext}\,Q_{rad} = T_{glass} - T_{sky} \tag{12}$$

with the external radiative thermal resistance, $R_{rad,ext}$,

$$R_{rad,ext} = 1/\left[\sigma\,\varepsilon_{glass}\,A_{abs}\,\left(T_{glass}^2 + T_{sky}^2\right)\left(T_{glass} + T_{sky}\right)\right] \tag{13}$$

where $T_{sky}$ is the "sky temperature" evaluated as in [12]

$$T_{sky} = 0.0552\,{T_{amb}}^{1/5} \tag{14}$$

The radiative solar energy rate absorbed by the plate, $Q_{abs}$, is

$$Q_{abs} = q_{abs}\,A_{abs} \tag{15}$$

where the fraction of the solar irradiance absorbed by the absorber plate, $q_{abs}$, is

$$q_{abs} = \eta\,G \tag{16}$$

with *G* the solar irradiance measured on a due south 30° inclined surface and $\eta$ the glass transmittance (0.90) times the absorber plate absorptance (0.94), that is assumed to be constant.

The energy balance on the heat transfer fluid gives

$$\frac{T_{abs} - T_{HTF,avg}}{R_{tot,HTF}} - \dot{V}_{HTF}\,\rho_{HTF}\,c_{HTF}\left(T_{HTF,out} - T_{HTF,in}\right) = \rho_{HTF}\,c_{HTF}\,V_{HTF}\,\frac{d\left(T_{HTF,avg}\right)}{dt} \tag{17}$$

with $T_{HTF,out}$ and $T_{HTF,in}$ the time varying temperatures of the HTF in the outlet and inlet sections of the collectors; $T_{HTF,avg} = (T_{HTF,out} + T_{HTF,in})/2$; $\dot{V}_{HTF}$, $\rho_{HTF}$, $c_{HTF}$, $V_{HTF}$, the volumetric flow rate, the density, the specific heat and the volume of the HTF in the collectors, respectively.

The thermal resistance between the HTF flowing in the tube and the absorber plate, $R_{tot,HTF}$, is evaluated taking into account only the contribution of the convective resistance and neglecting the far smaller conductive resistances in the tube and the absorber plate walls

$$R_{tot,HTF} = 1/\left(\bar{h}_{tube}\,A_{i,tube}\right) \tag{18}$$

where $A_{i,tube}$ is the area of the inner surface of the tube and $\bar{h}_{tube}$ is the mean convective heat transfer coefficient

$$\bar{h}_{tube} = \left(\overline{Nu}_{tube}\,k_{HTF}\right)\,{D_{i,tube}}^{-1} \tag{19}$$

with $k_{HTF}$ the thermal conductivity of the HTF; $D_{i,tube}$ the inner diameter of the tube; $\overline{Nu}_{tube}$ the mean Nusselt number evaluated using the correlation for thermally fully developed laminar flow in ducts, the Reynolds number being lower than 2300.

The term $\dot{V}_{HTF}\,\rho_{HTF}\,c_{HTF}\left(T_{HTF,out} - T_{HTF,in}\right)$ in equation (17) represents the heat rate delivered to the coil heat exchanger, $Q_{useful}$.

Each collector has circular distributor pipes, with a diameter of $2.2 \cdot 10^{-2}$ m, in the HTF entrance and exit sections. Their contribution to the heat transfer from the absorber to the HTF was also considered.

The energy balances on the overall collector and on the glass give, respectively,

$$Q_{abs} = Q_{up} + Q_d + Q_{useful} + \sum_k V_k \, \rho_k \, c_k (dT_k/dt) \tag{20}$$

$$Q_{up} = Q_{conv,up} + Q_{rad} + V_{glass} \, \rho_{glass} \, c_{glass} \left(dT_{glass}/dt\right) \tag{21}$$

with $V_k$, $\rho_k$, $c_k$ and $T_k$ the volume, the density, the specific heat and the temperature of each component of the collector (absorber plate, back box cover, tube, air). The thermal capacitance of each component in equation (20) has been modelled for each component of the collector. The reference temperatures for the tube, the insulation and the air layer have been chosen equal to the absorber plate temperature, the arithmetic mean of the absorber and the box back cover temperatures, and the arithmetic mean of the absorber plate and the glass temperatures, respectively. The first order backward discretization of the time derivative has been applied.

At each time-step, the system of equations (1, 3, 5, 10, 12, 15, 17, 20, 21) is solved implicitly. The input temperature of the HTF at the inlet of the first collector is given by the coil heat exchanger simulation, while the HTF temperature at the inlet of the second collector is assumed equal to the HTF temperature at the outlet of the first collector. The model outputs are the time-variable temperatures of all the collectors components and the time-variable HTF temperature at the exit of the collectors tubes.

*2.2. Immersed coil heat exchanger model*

A transient one-dimensional model has been developed for the evaluation of the temperature field in the HTF flowing through the immersed coil heat exchanger. The data of the enameled crude steel coil heat exchanger that has been considered in the present study are reported in Table 2.

The heat exchanger has been subdivided into *I* isothermal nodes, having the same volume. The energy balance equation for the *i*th node is

$$\rho_{HTF,i} \; c_{HTF,i} \, V_{HTF,i} \frac{dT_{HTF,i}}{dt} = \frac{T_{w,tank} - T_{HTF,i}}{R_{coil}} + \rho_{HTF,i} \, c_{HTF,i} \, \dot{V}_{HTF,i} \left(T_{HTF\,in,i} - T_{HTF_{out,i}}\right) \tag{22}$$

where $\rho_{HTF,i}$ and $c_{HTF,i}$ are the density and the specific heat of the HTF at the *i*th node, respectively; $V_{HTF,i}$ is the volume of the *i*th node; $T_{w,tank}$ is the time and space varying temperature of the water inside the tank; $\dot{V}_{HTF,i}$is the volumetric flow rate in the *i*th node; $T_{HTF\,in,i}$ and $T_{HTF\,out,i}$ are the time varying HTF inlet and outlet temperatures at the boundaries of the *i*th node, respectively;

The thermal resistance between the HTF in the coil heat exchanger and the water in the tank, $R_{coil}$, is

$$R_{coil} = R_{conv,i_{coil}} + R_{conv,e_{coil}} + R_{cond} \tag{23}$$

The internal convective thermal resistance, $R_{conv,i_{coil}}$, is given by

$$R_{conv,i_{coil}} = 1/\left(A_{i,coil} \, \bar{h}_{conv,i_{coil}}\right) \tag{24}$$

**Table 2.** Immersed coil heat exchanger data.

| | |
|---|---|
| Thermal conductivity | 40.0 W/m K |
| Inner diameter | $3.0 \cdot 10^{-2}$ m |
| Outer diameter | $3.4 \cdot 10^{-2}$ m |
| Helix diameter | $44.0 \cdot 10^{-2}$ m |
| Helix height | $75.0 \cdot 10^{-2}$ m |
| Helix length | 16.63 m |
| Helix outer area | 1.76 $m^2$ |

where $A_{i,coil}$ is the area of the internal surface of each node of the coil and $\bar{h}_{conv,i_{coil}}$ is the mean internal convective heat transfer coefficient

$$\bar{h}_{conv,i_{coil}} = \left(\overline{Nu}_{i_{coil}}\, k_{HTF}\right)/D_{i,coil} \tag{25}$$

with $\overline{Nu}_{i_{coil}}$ the mean Nusselt number, evaluated using the Gnielinski's correlation for a coiled tube heat exchanger [13], and $D_{i,coil}$ the inner diameter of the coil.
The external convective thermal resistance, $R_{conv,e_{coil}}$, is given by

$$R_{conv,e_{coil}} = 1/\left(A_{e,coil}\, \bar{h}_{conv,e_{coil}}\right) \tag{26}$$

where $A_{e,coil}$ is the area of the external surface of each node of the coil and $\bar{h}_{conv,e}$ is the mean external convective heat transfer coefficient

$$\bar{h}_{conv,e_{coil}} = \left(\overline{Nu}_{e_{coil}}\, k_{w,tank}\right)/D_{e_{coil}} \tag{27}$$

with $D_{e_{coil}}$ the outer diameter of the coil, $k_{w,tank}$ the thermal conductivity of the water inside the tank and $\overline{Nu}_{e_{coil}}$ the mean Nusselt number evaluated with the Morgan's correlation for natural convection over horizontal cylinders [14].

The conductive thermal resistance of the coil has been neglected, since it is negligible compared with the internal and external convective thermal resistances.

For each time-step and for each node, equation (22) is solved using the implicit Euler method. The input for the numerical simulation of the HTF inside the coil are the HTF temperature at the inlet section, that has been considered equal to the HTF temperature at the outlet of the second collector, and the temperature distribution of the water inside the tank. The output of the model is the time-variable HTF outlet temperature at each node.

*2.3. Heat storage tank model*

A vertical cylindrical heat storage tank has been considered in the present study. The inner tank diameter is 0.58 m and its height is $H_{tank}$ = 1.5 m, with a 0.40 m$^3$ volume. The thermal insulation consists of a 50 mm thick polyurethane layer. The inlet section of the immersed coil heat exchanger is located on the tank side wall, 0.75 m above the tank bottom, while the outlet section is at the tank bottom. No water inlet or outlet and no auxiliary heaters have been simulated. Figure 3 shows the temperature array used for the simulation of the storage tank.

The water is subdivided into *J* isothermal nodes, each representing an equal volume water layer. The energy balance for the *j*th node can be written as

$$\rho_{w,j}\ \ c_{w,j}\, V_{w,j}\, \frac{dT_{w,j}}{dt} = \frac{T_{HTF} - T_{w,j}}{R_{coil}} + Q_{cond} - \frac{T_{w,j} - T_{amb}}{R_{tank}} \tag{28}$$

where $\rho_{w,j}$, $c_{w,j}$, $V_{w,j}$ and $T_{w,j}$ are the density, the specific heat, the volume, and the temperature of each water layer, respectively; $T_{HTF}$ is the time and space varying temperature of the water inside the coil; $Q_{cond}$ is the conductive heat rate between the *j*th layer and the adjacent water layers, that is the sum of the following two contributions

$$Q_{cond} = \frac{\pi D_{i_{tank}}^2}{4}\frac{k_{w\,tank}}{\Delta_l}\left(T_{j-1} - T_j\right) + \frac{\pi D_{i_{tank}}^2}{4}\frac{k_{w\,tank}}{\Delta_l}\left(T_{j+1} - T_j\right) \tag{29}$$

where $D_{i,tank}$ is the inner tank diameter and $\Delta_l$ is the distance between two adjacent nodes.
The thermal resistance of each layer of the tank wall, $R_{tank}$, was evaluated as

$$R_{tank} = R_{conv,i_{tank}} + R_{cond_{tank}} + R_{conv,e_{tank}} \tag{30}$$

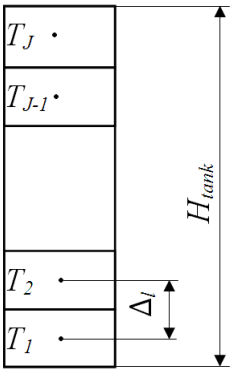


**Figure 3.** Temperatures array for the heat storage tank simulation.

where the inner convective resistance, $R_{conv,i_{tank}}$, is

$$R_{conv,i_{tank}} = 1/\left(A_{i_{tank}}\,\bar{h}_{conv,i_{tank}}\right) \quad (31)$$

with $A_{i_{tank}}$ the area of the inner lateral surface of each layer and $\bar{h}_{conv,i_{tank}}$ the mean convective coefficient at the inner tank wall, which was evaluated with the correlation for natural convection on a vertical flat plate.

The conductive thermal resistance of the tank wall, $R_{cond_{tank}}$, was evaluated as

$$R_{cond_{tank}} = \ln\left(r_{o_{tank}}/r_{i_{tank}}\right)/\left(2\,\pi\,k_{ins_{tank}}\,\Delta_l\right) \quad (32)$$

where $r_{o_{tank}}$ and $r_{i_{tank}}$ are the outer and the inner radius of the tank, respectively, and $k_{ins,tank}$ is the thermal conductivity of the insulation. The tank thickness was assumed to be equal to the insulation thickness, since the conductive thermal resistance of the tank steel was neglected.

The convective thermal resistance at the external wall of the tank, $R_{conv,e_{tank}}$, is given by

$$R_{conv,e_{tank}} = 1/\left(A_{e_{tank}}\,\bar{h}_{conv,e_{tank}}\right) \quad (33)$$

where $A_{e_{tank}}$ is the external lateral area of each layer of the tank and $\bar{h}_{conv,e_{tank}}$ is the mean convective heat transfer coefficient at the external wall of the tank, that was set equal to 5 W/m$^2$ K. For each time-step, the system of energy balance equations (29) is solved using the implicit Euler method. The empirical reversion-elimination algorithm [15, 16] was adopted, in order to account for the effects of natural convection between the water layers at different heights in the thermal stratification inside the tank. Indeed, at each time-step, should an unstable gradient arise, namely when a node temperature becomes higher than the temperature of the adjacent above node, the mixing of the fluid in the two layers occurs. The mixing process continues until the above layer is warmer than the below mixed layers. Then, the algorithm goes bottom-down to allow layers to mix with the warmer layers below. The input for the heat storage tank model are the ambient temperature and the HTF temperatures.

### *2.4. Components coupling*

The solar DHW system was simulated numerically by means of a Matlab home-made code. Heat losses through the piping walls have been neglected. The system components were coupled with an iterative approach. At each time step, the first collector is simulated by using as input temperature at its inlet section the HTF temperature at the exit of the coil heat exchanger at the previous time-step. Then, the second collector is simulated using as input temperature at its inlet section the updated value of the HTF temperature at the first collector outlet. The coil heat exchanger is simulated using as input temperature at its inlet section the HTF temperature at the exit section of the second collector, given by the above described simulation of the collectors; the temperature distribution in the tank water is that evaluated in the previous time step. Finally, the tank is simulated using the updated temperatures of the HTF inside the coil heat exchanger. Then the process restarts from the collectors simulation using the updated temperatures and goes on till convergence is attained.

## 3. Simulations results

The results of a one-day simulation of the solar DHW system are presented in the following,. The input time-varying ambient temperature and solar irradiance, measured at the ENEA Portici RC, as a function of the hours of the day are reported in figure 4. The HTF flow rate was set equal to $6.0 \cdot 10^{-5}$ m$^3$/s and a 60 s time step was used. The initial temperatures of the collectors components were set

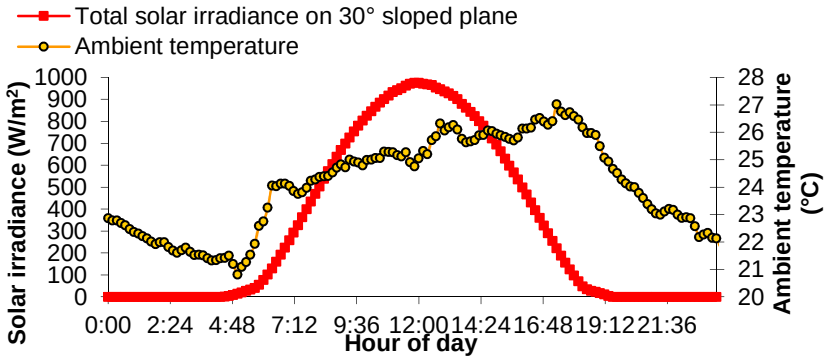


**Figure 4.** Solar irradiance and ambient temperature *vs.* hour of the day.

equal to the ambient temperature at midnight, while the initial temperatures of the water in the tank and of the HTF in the heat exchanger were chosen equal to 18°C, that is the average temperature of mains water in July at Portici.

The HTF temperature in the heat exchanger inlet and outlet sections as well as the mean water tank temperature as a function of the hour of the day are reported in figure 5. Since the heat losses through the piping system have been neglected, the HTF temperature at the heat exchanger inlet coincides with the HTF temperature in the second collector outlet section and the HTF temperature in the heat exchanger outlet section is the same as the HTF temperature at the first collector inlet section.

As it was to be expected, the HTF and water temperatures undergo a strong increase after the sunrise and, due to the thermal inertia of solar collectors, the maximum value of the HTF temperature in the inlet section of the heat exchanger is attained at about 14.00. It is worth noticing that the temperature of the HTF in the inlet section of the heat exchanger and the mean temperature of the water tank become equal at about 18.00. Afterwards, till midnight, the HTF circulation is switched off to avoid heat transfer from the heat storage tank to the solar collectors, and the HTF temperature in the heat exchanger is assumed equal to the mean water temperature. The slight decrease in the mean water temperature when there is not the HTF circulation is due to the heat losses through the tank walls.

Figure 6 shows the collectors components temperatures, the mean HTF temperature in the tube, and the ambient temperature during the day. Before sunrise, the temperatures of the external components of each collector, namely the box and the glass, are nearly equal to the ambient temperature. The

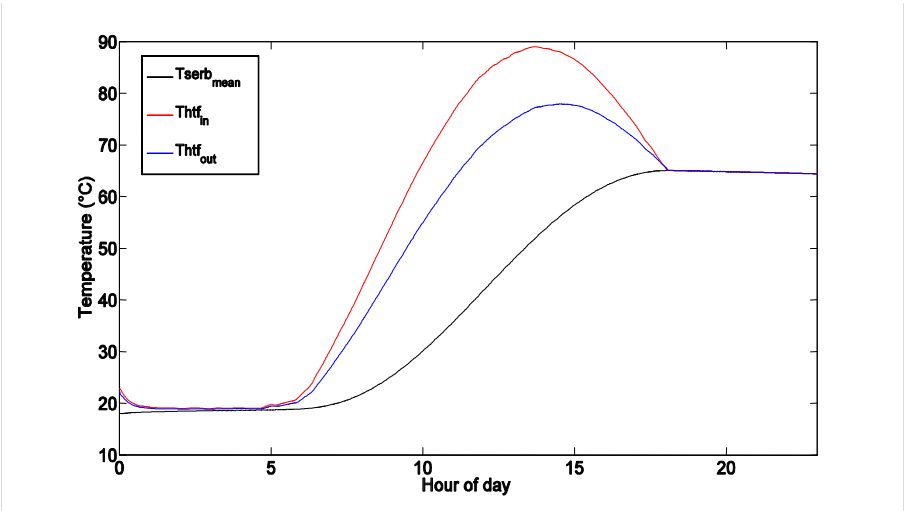


**Figure 5.** HTF temperature in the heat exchanger inlet and outletsections and mean water tank temperature *vs.* the hour of the day.

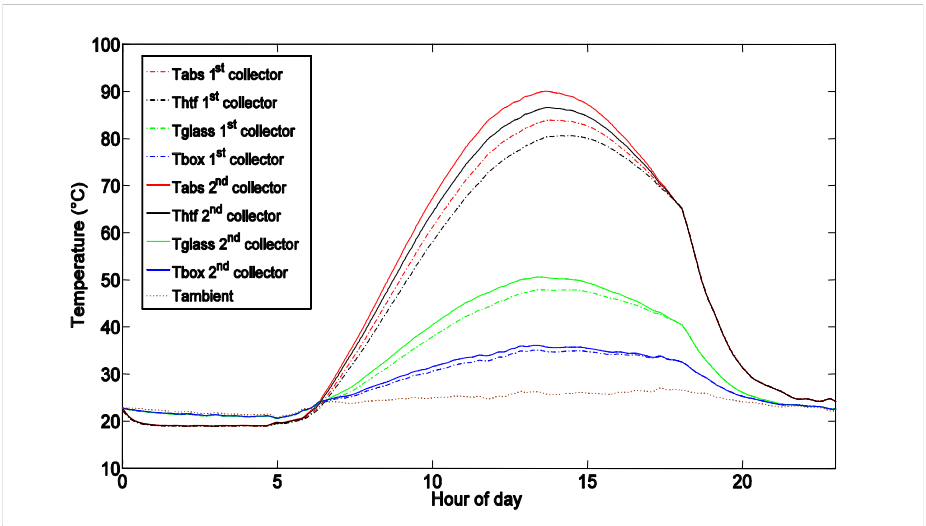


**Figure 6.** Collectors components temperatures, mean HTF temperatures in the tube, and ambient temperature *vs*. the hour of the day.

temperatures of the absorbers and of the heat transfer fluids are lower than the ambient temperature, since the initial temperature of the tank water is lower than the ambient temperature, and also because of the thermally resistive layers in the collectors. The above layers consist of the insulation and the air gap that separate the tube and the absorber from the box and the glass, respectively. The hour at which the HTF circulation switches off can be easily seen in figure 6, which points also out a strong decrease in the temperature of the collector components due to the energy losses to the ambient.

The useful heat rate and the heat rate dissipated at the top and bottom sides of the collectors are reported in figure 7. It can be noticed that the useful heat rate attains the maximum value at the same time, when the solar irradiance is the maximum. Figure 5 showed that the HTF temperature in the inlet section of the first collector becomes slightly higher than the outlet temperature in the second collector at the switch-off time. This is the reason why the useful heat rate becomes negative at the switch-off time, as shown in figure 7. Due to the larger heat losses from the second collector, the useful heat rate is higher in first collector until 16.30. Afterwards the useful heat rate in the second collector becomes slightly higher, due to the larger thermal energy stored in the absorber plate and pipes.

The collectors efficiency, that is the ratio of the collector useful heat rate to the solar irradiation on

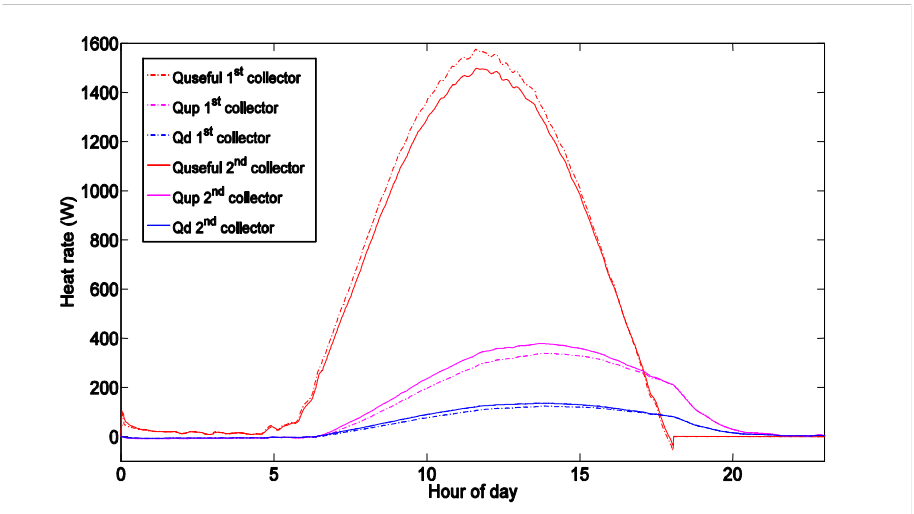


**Figure 7.** Collectors useful and dissipated heat rates *vs*. the hour of the day.

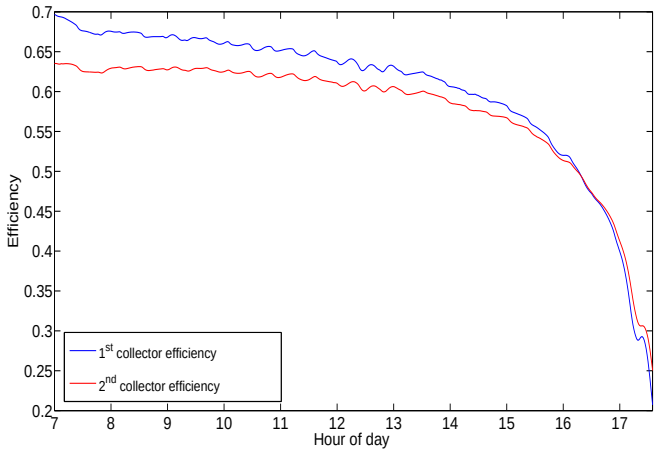


**Figure 8.** Collectors efficiency.

the collector, as a function of the hour of the day, is reported in figure 8. It can be noticed that for the same reason, again at about 16.30 the efficiency of the second collector becomes higher than that of the first collector.

## 4. Conclusions

The numerical simulation of a solar DHW system, made up by two flat plate solar collectors, a vertical cylindrical water tank for the heat storage and an immersed coil heat exchanger, has been addressed. Mathematical models and numerical schemes for each system component, described in the paper, were implemented in a Matlab home-made code, allowing the numerical simulation of the system.

Results of the simulation performed using as input data the ambient temperature and the solar irradiance at the ENEA Portici Research Center in a summer day were presented and discussed.

## 5. References

[1] Rodríguez-Hidalgo M C, Rodríguez-Aumente P A, Lecuona A, Legrand M and Ventas R 2012 Appl. Energy **97** 897-906.
[2] Dehghan A A and Barzegar A 2011 Energy Conversion and Management **52** 468-76.
[3] Kenjo L, Inard C and Caccavelli D 2007 Appl. Thermal Engineering **27** 1986-95.
[4] Klein S A, Duffie J A and Beckman A 2010 J. Engineering Gas Turb.Power **96** 109-13.
[5] Rodrìguez-Hidalgo M C, Rodriguez-Aumente P A, Lecuona A, Gutìerrez-Urueta G L and Ventas R 2011 Appl. Thermal Engineering **31** 2394-404.
[6] Rodrìguez-Hidalgo M C, Rodriguez-Aumente P A, Lecuona A, Gutìerrez-Urueta G L and Ventas R 2011 Appl. Thermal Engineering **31** 2385-393.
[7] Cadafalch J 2009 Solar Energy **83** 2157-64.
[8] Logie W R and Frank E 2013 J. Solar Energy Engineering **135** 1-7.
[9] Chauvet L P and Nevrala D J 1993 Appl. Energy **44** 283-314.
[10] Bejan, A and Kraus A D 2003 *Heat Transfer Handbook*, John Wiley & Sons Inc. Hoboken, NJ
[11] Hollands K G T, Unny T E, Raithby G D and Konicek L 1976 J. Heat Transfer **98** 189–193.
[12] Ashrae HVAC 1999 *Application Handbook*,.
[13] Gnielinski Y 1986 *Heat Transfer 1986*, San Francisco, USA, pp. 2847-54.
[14] Morgan V T 1975 *Adv. Heat Transfer*, vol 11, pp. 199-264.
[15] Mather D W, Hollands K G T and Wright J L 2002 Solar Energy **73** 3-13.
[16] Newton B J, Schmid M, Mitchell J W and Beckman W A 1995 Proc. ASME/JSME/JSME Int. Solar Energy Conf., March 19-24 Maui, Hawaii. ASME, New York, Part 2; 1111.